J. Fluid Mech. (2009), *vol.* 633, *pp.* 99–114.
doi:10.1017/S0022112009007459 Printed in the United Kingdom

Unsteady two-layer hydraulic exchange flows with friction

S. S. LI[1]† AND G. A. LAWRENCE[2]

[1]Department of Building, Civil and Environmental Engineering, Concordia University, Montreal, Quebec, Canada H3G 1M8

[2]Department of Civil Engineering, University of British Columbia, Vancouver, BC Canada V6T 1Z4

(Received 7 December 2008 and in revised form 12 February 2009)

Two-layer exchange flow through a contraction with both friction and barotropic forcing is modelled in terms of three parameters reflecting the friction and the strength and period of the barotropic forcing. In the appropriate limits, the results for steady flow with and without friction, and inviscid barotropically forced flow are recovered. The predicted time-dependent interface position compares well with laboratory experiments, improving on the inviscid formulation. The concurrent effects of friction and barotropic forcing on average exchange flow rate are determined. When friction is weak barotropic forcing increases the exchange rate. However, when friction is high, tidal forcing can result in a reduced exchange rate, a phenomena that we call tidal inhibition. When friction is weak maximal exchange occurs throughout the tidal cycle, but as friction is increased submaximal flow develops for longer and longer periods. As friction is increased even further the flow becomes hydraulically uncontrolled. The parameter range for major sea straits includes tidally enhanced and tidally inhibited flows, as well as maximal, submaximal and uncontrolled flows.

1. Introduction

Exchange flows often occur in natural straits and man-made channels that connect two water bodies of different density. Well-known examples include the exchange between the Atlantic Ocean and the Mediterranean Sea through the Strait of Gibraltar (Armi & Farmer 1988; Farmer & Armi 1988), between the Sea of Marmara and the Black Sea through the Bosphorus (Gregg & Ozsoy 2002) and between the North Sea and the Baltic Sea through the Great Belt (Ottesen-Hansen & Moller 1990). In the absence of time-dependent forcing and with negligible fluid mixing, the density-driven exchange can be treated as two steady counter-flowing homogeneous layers (figure 1*a*, *b*).

In many circumstances, density-driven exchange is influenced by tidal forcing. In the Strait of Gilbraltar tidal currents flowing over uneven topography trigger barotropic waves (Morozov *et al.* 2002), significantly affecting the exchange through the strait. Similarly, the exchange flow through the Bab el Mandab Strait is influenced by energetic tidal currents entering the strait (Jarosz, Murray & Inoue 2005). Barotropic forcing can also be associated with basin-scale seiches. In Lake Ontario, surface

† Email address for correspondence: samli@bcee.concordia.ca.

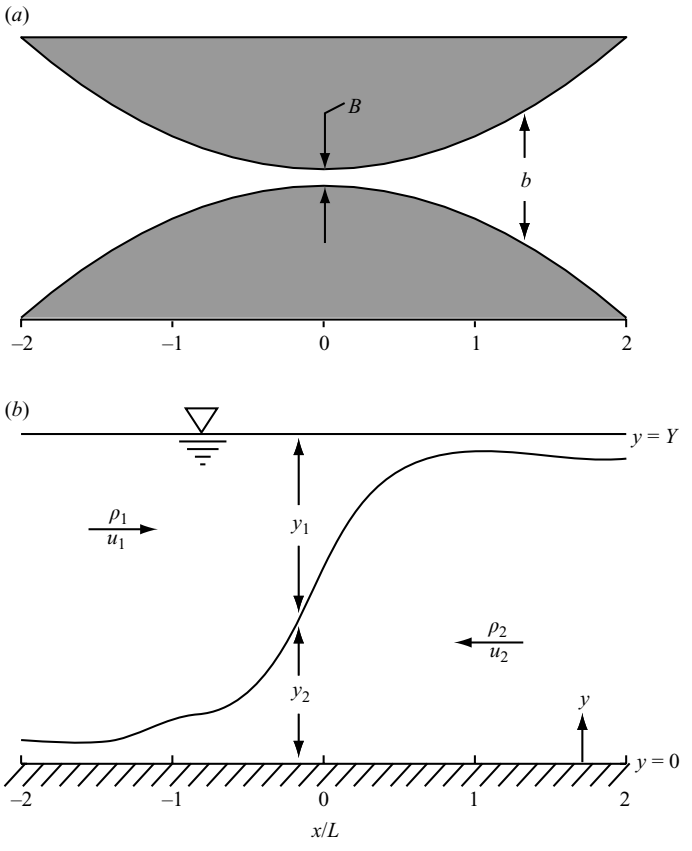

FIGURE 1. Definition diagram for two-layer exchange flow through a contraction: (*a*) top view; (*b*) side view.

seiches at multiple frequencies are triggered by wind forcing, resulting in an unsteady exchange through the Burlington Ship Canal (Lawrence *et al.* 2004).

Exchange flows, whether they are steady or unsteady, are inevitably subject to friction. For instance, field data show that friction on the bottom and sidewalls of the Burlington Ship Canal combines with interfacial shear, to reduce the exchange flow rate to approximately 50 % of the inviscid value (Lawrence *et al.* 2004).

Exchange flow through a contraction has been the subject of a series of investigations. Armi (1986) considered the frictionless case without forcing. Armi & Farmer (1986) and Farmer & Armi (1986) analysed frictionless exchange with quasi-steady forcing. Helfrich (1995) and Frankcombe & Hogg (2007) analysed frictionless exchange with periodic forcing. Zhu & Lawrence (2000) and Zaremba, Lawrence & Pieters (2003) investigated frictional effects without barotropic forcing. While both friction and barotropic forcing have been included in numerical models of specific straits (Oguz, Ozsoy & Latif 1990), the present study may be the first general study of the exchange flow problem to include both friction and barotropic forcing. The theoretical background to this problem is presented in § 2, followed by a description of solution techniques and test runs in § 3. In § 4, we present predictions of interface position, exchange flow rate and flow regime. The results are discussed in § 5 and conclusions are drawn in § 6.

2. Theoretical background

Following Helfrich (1995) we consider exchange flow through a contraction of width:

$$b(x) = B\left[1 + 4\left(\frac{x}{L}\right)^2\right] \tag{2.1}$$

where B is the width at the narrowest point, x is the horizontal distance from this point and L is the horizontal length scale (figure 1*a*). This shape allows us to focus on the effects of friction and barotropic forcing, while avoiding the complications arising from a more complex geometry.

Four main approximations are made to simplify this problem. First is the assumption of no fluid mixing across the density interface, ensuring the density within each layer remains constant. Second, hydrostatic pressure is assumed. Third, the flow is assumed to be one-dimensional, with layer velocities varying only in the flow direction. Finally, a small relative density difference between the layers allows us to assume that variations in free surface elevation are small and to focus on variations in interface height.

We do not attempt to model the processes that result in interfacial shear, but retain their gross effect on the momentum balance of the flowing layers using the quadratic law. Bottom friction and sidewall friction are treated similarly. With these simplifications, two-layer exchange is completely described by the interface height and the layer velocities. Following Zaremba *et al.* (2003), we can write the equation of mass conservation and the momentum equation for each layer as follows:

$$\frac{\partial a_j}{\partial t} + \frac{\partial (a_j u_j)}{\partial x} = 0, \tag{2.2}$$

$$\frac{\partial u_j}{\partial t} + \frac{\partial}{\partial x}\left[\frac{u_j^2}{2} + g(y_1 + y_2) - (j-1)g' y_1\right] = g' S_j, \tag{2.3}$$

$$S_j = (1-j)\frac{f_b}{2}\frac{u_j|u_j|}{g' y_j} - f_w \frac{u_j|u_j|}{g' b} - (-1)^j \frac{f_i}{2}\frac{\Delta u|\Delta u|}{g' y_j}, \tag{2.4}$$

where subscript, $j = 1(2)$, refers to the upper (lower) layer; a_j and y_j denote the layer area and thickness, which are related through $y_j = a_j/b$; u_j is the layer velocity; t is time; the reduced gravitational acceleration $g' = g(\rho_2 - \rho_2)/\rho_2$, where ρ_j represents layer density; S_j is the friction slope. In (2.4), $\Delta u = u_2 - u_1$ is the velocity shear; and f_w, f_b and f_i are the wall, bottom and interfacial friction factors, respectively.

Following Helfrich (1995) we introduce barotropic forcing via a volumetric transport of fixed frequency and amplitude

$$q = q_o \sin\left(\frac{2\pi t}{T}\right), \tag{2.5}$$

where $q = u_1 a_1 + u_2 a_2$ is the barotropic transport, q_o is the amplitude and T is the period. Next, we rewrite (2.2) and (2.3) in terms of Δu and a_1; the layer velocities can be recovered from $u_1 = [(q + a_1 \Delta u)/a] - \Delta u$ and $u_2 = \Delta u + u_1$, where $a = a_1 + a_2$ is the total cross-sectional area. Non-dimensional equations for Δu and a_j are obtained using the following time, length and velocity scales: $t^* = t/T$, $x^* = x/L$, $y_j^* = y_j/Y$, $b^* = b/B$, $\Delta u^* = \Delta u/\sqrt{g'Y}$, $u_j^* = u_j/\sqrt{g'Y}$ and $q^* = q/(u_o Y B)$, where $Y = y_1 + y_2$ is the total flow depth; and u_o is the amplitude of the barotropic flow speed at the narrows. The asterisks indicate dimensionless quantities. Equations (2.2), (2.3) and (2.4) reduce

Strait	Y (m)	L (km)	g' (m s^{-2})	$\sqrt{g'Y}$ (m s^{-1})	u_o (m s^{-1})	α	β	γ	q_{FA86}	q_{Z03}	q_e
				Low friction							
Tiran	270	3	0.0035	0.97	0.24	0.04	0.25	15	1.0	0.94	0.95
				Moderate friction							
Gibraltar	280	20	0.02	2.4	1.5	0.3	0.6	5.3	0.73	0.49	0.62
Lombok	350	40	0.05	4.2	2.1	0.5	0.5	4.7	1.0	0.63	0.66
Messina	80	10	0.01	0.89	1.8	0.5	2.0	4.0	1.0	0.63	1.12
Bab El Mandab	137	20	0.033	2.1	0.5	0.6	0.24	4.8	1.0	0.58	0.59
				High friction							
Oslofjord	15	10	0.02	0.55	0.6	2.7	1.0	2.5	1.0	0.30	0.23
Bosphorus	35	30	0.12	2.0	0.5	3.4	0.25	3.1	1.0	0.27	0.25

TABLE 1. Geometry and dynamic parameters corresponding to some prominent straits assuming $f_b = 0.004$ and $r_i = 1$. Values of Y, L, g', u_o and T ($= 12.5$ h) are those given in Helfrich (1995), except for Bab el Mandab where the values of Smeed (2004) are used. All straits are idealized as contractions except for Gibraltar which is treated as an offset sill and contraction, with depth 280 m at the sill and 560 m in the contraction, and the width at the narrows of 0.8 times the width at the sill. q_{FA86}, q_{Z03} and q_e are the exchange rates predicted by Farmer & Armi (1986), Zaremba *et al.* (2003) and the present study, respectively.

to

$$\frac{\partial a_1}{\partial t} + \gamma \frac{\partial}{\partial x}\left(\frac{\beta q a_1 + a_1^2 \Delta u}{a} - a_1 \Delta u\right) = 0 \tag{2.6}$$

$$\frac{\partial \Delta u}{\partial t} + \gamma \frac{\partial}{\partial x}\left(\frac{\beta q \Delta u + a_1 \Delta u^2}{a} - \frac{\Delta u^2}{2} - y_1\right) = \gamma\alpha\left(\frac{u_2|u_2|}{2y_2} + \gamma_i \frac{y\Delta u|\Delta u|}{2y_1 y_2} + \gamma_w \frac{u_2|u_2| - u_1|u_1|}{b}\right) \tag{2.7}$$

where the asterisks have been dropped.

Five dimensionless parameters appear in (2.6) and (2.7)

$$\alpha = \frac{f_b L}{Y}; \quad \beta = \frac{u_o}{\sqrt{g'Y}}; \quad \gamma = \frac{T\sqrt{g'Y}}{L} \tag{2.8}$$

$$r_i = \frac{f_i}{f_b}; \quad r_w = \frac{f_w Y}{f_b B}. \tag{2.9}$$

Unless otherwise stated we set r_i to unity and r_w to zero. The three primary parameters can be interpreted as follows:

(1) α gives the relative importance of frictional to inertial effects;

(2) β gives the strength of the barotropic flow relative to the velocity scale of the density-driven flow and

(3) γ represents the ratio of the forcing period to the time scale for interface waves to travel through the strait.

We investigate a range of values of α, β and γ representative of conditions in the well-known straits, listed in table 1.

3. Solution techniques and test runs

The MacCormack explicit multistep method (Chung 2002, p. 82) is used to solve (2.6) and (2.7) numerically. This finite difference method employs a predictor-corrector

scheme well suited for nonlinear problems. This scheme handles anticipated hydraulic jumps well, with little distortion when the Courant number, $C = u_{max}\Delta t/\Delta x$, is close to one, where u_{max} is the maximum velocity, Δt is the time step and Δx is the grid resolution. The scheme is of second-order accuracy, and numerically stable for $C \leqslant 1$.

Solving the nonlinear problem numerically requires the addition of a small amount of diffusion to maintain stability. Otherwise, high frequency short waves appear at the interface due to truncation errors in the second-order numerical technique. Physically, disturbances shorter than a critical wavelength are subject to the Kelvin–Helmholtz instability (see Drazin & Reid 1981). This critical wavelength increases with increasing velocity shear. Following Helfrich (1995) and Zaremba *et al.* (2003) we limit the growth of unstable waves by adding a diffusion term to the right-hand side of (2.6) and (2.7). The viscosity in this diffusion term is set as low as possible, typically making the diffusion term three orders of magnitude lower than the other terms in (2.6) and (2.7).

The above approach is acceptable if Long's (1956) criterion, i.e. $|\Delta u| \leqslant 1$, is satisfied. Otherwise disturbances of all wavelengths may become unstable and solutions to (2.6) and (2.7) may not be valid. Lawrence (1990) demonstrated that $(\Delta u)^2 \leqslant G^2$ in all two-layer flows, so Long's criterion is always satisfied in regions of internally subcritical flow. In our simulations Long's criterion was always satisfied throughout the domain when $\alpha \geqslant 0.1$. For $\alpha \leqslant 0.1$ Long's criterion was often violated in the supercritical flow downstream of the throat of the contraction during part of the tidal cycle. Even this case is generally not a problem, since instabilities are swept away from the throat. Except where noted, we have only considered flows where Long's criterion is satisfied.

In reality interfacial shear instabilities evolve to form a mixed layer of thickness $\delta \approx 0.3(\Delta u)^2 Y$ (Koop & Browand 1979). Assuming $|\Delta u| = 1$, the upper bound in regions of subcritical flow, Helfrich (1995) demonstrated that the presence of a mixed layer reduces the exchange flow through a contraction by approximately 20 %. This reduction in exchange is based on the characteristic shape of the velocity and density profiles in flows subject to interfacial mixing and, to a first approximation, is independent of other processes, e.g. barotropic forcing. A comparable reduction of 10–15 % was obtained by Winters & Seim (2000) using a numerical model of exchange through a contraction that resolved interfacial shear instabilities. Hogg, Ivey & Winters (2001) consider exchange flows with much higher reductions in exchange rate, but such flows require stronger mixing than that generated by interfacial shear instabilities. While we acknowledge the importance of interfacial mixing, its inclusion is beyond the scope of the present study, and we assume that the two-layer approximation does not compromise our ability to investigate the effects of friction and tidal forcing.

At the ends of the channel an explicit radiation condition (Orlanski 1976) is applied to a_1 and Δu. While our focus is on the dimensionless range $[-3, 3]$, we place the channel ends at $x \approx 5$ to avoid possible artificial end effects. The radiation condition allows waves to propagate freely across the open boundaries of a frictionless strait. For dynamic consistency, we introduce a ramping factor between 0 and 1 for friction over the channel sections $[-5, -4]$ and $[4, 5]$; the factor allows zero friction at the channel ends and linearly ramps up to the values given by the right-hand side of (2.7) at $x = \pm 4$.

The integration of (2.6) and (2.7) proceeds from a lock-exchange initial condition, where initially a barrier at the narrowest section ($x = 0$) separates the two water bodies of different density. The barrier is then removed releasing gravity currents that propagate away from the narrows. The equations are integrated for one tidal cycle before imposing barotropic forcing. Barotropic forcing is then imposed for at least 10

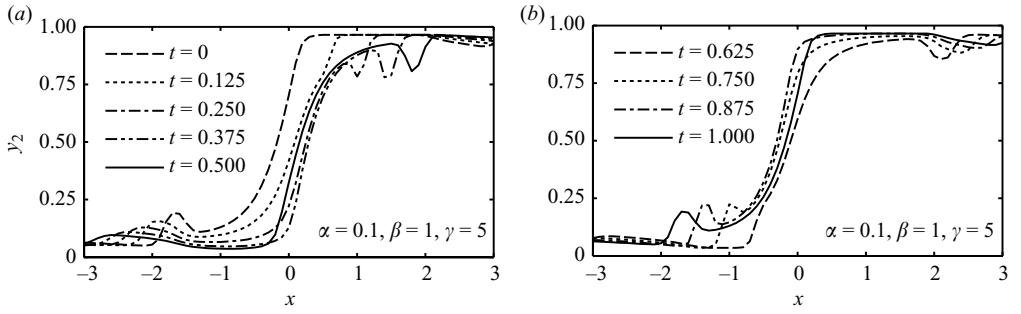

FIGURE 2. Predicted unsteady profiles of the density interface over a barotropic forcing cycle. (*a*) The predictions at various stages during the first half of the forcing cycle, when the barotropic transport [given by (2.5)] is from left to right. (*b*) The predictions during the second half of the forcing cycle, when the transport is from right to left. Internal hydraulic jumps form near the contraction on both sides and propagate towards the ends of the channel. The hydraulic jumps become weaker as they propagate because of channel expansion.

tidal cycles to attain stable periodic solutions of interface position and layer velocities. The lock-exchange initial condition allows maximal exchange flows with hydraulic controls on either side of the narrows. Depending on the parameter values, maximal exchange may persist throughout the simulation, or one or both of the controls may be lost resulting in submaximal or uncontrolled exchange, respectively.

To test the model a flow with weak friction ($\alpha = 0.1$) and moderate barotropic forcing ($\beta = 1$ and $\gamma = 5$) was chosen. This set of friction and forcing parameters yielded fast-moving interfacial waves and hydraulic jumps (figure 2*a*, *b*). About one-quarter of the way through each tidal cycle hydraulic jumps form at $x \approx -1$ and are swept downstream (from left to right) by the barotropic flux. The corresponding behaviour starts at $x \approx -1$ about three-quarters of the way through each tidal cycle. On both sides of the contraction the hydraulic jumps weaken as they propagate in the expanding channel. Over the entire forcing cycle, there is no detectable reflection from the ends. The ability of the model to obtain stable solutions and to track hydraulic jumps without boundary reflection provided the confidence needed to proceed with an investigation of the effects of varying α, β and γ.

4. Results

This section compares predicted interface positions with the laboratory experiments of Helfrich (1995). It also investigates the variation of interface position, exchange flow rate and flow regime, for a range of values of α, β and γ representative of flows found in nature.

4.1. *Comparison with laboratory experiments*

Helfrich (1995) conducted laboratory experiments in a channel satisfying (2.1) with $B = 0.05\,\mathrm{m}$ and $L = 0.2\,\mathrm{m}$ for $|x| \leqslant 0.5$. He presents photographs of an experiment where the total flow depth was $Y = 0.09\,\mathrm{m}$, $\beta = 1$ and $\gamma = 7.8$, and provides inviscid predictions of the interface profile at various stages of a forcing cycle (figure 3*a–h*). We have made a corresponding set of frictional predictions using $\alpha = 0.04$, $r_i = 0.5$ and $r_w = 1.8$. These values were obtained by setting $f_b = f_w = 0.02$ and $f_i = 0.01$, based on the study of Zhu & Lawrence (2000). While these friction factor estimates are subject to considerable error, the predictions of interface profiles are not particularly

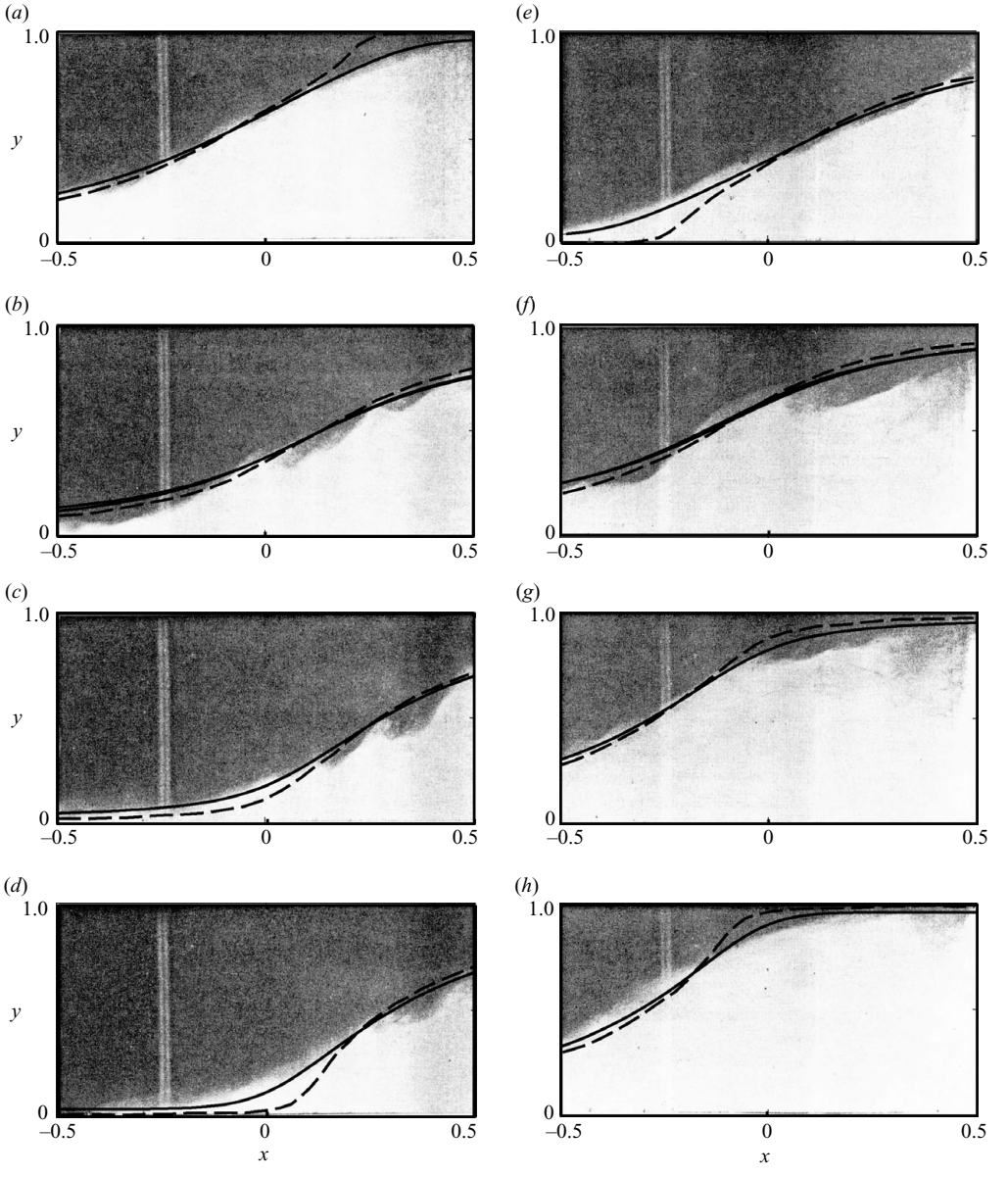

FIGURE 3. Snapshots of cyclic interface profiles at eight different stages of a forcing cycle. Adjacent stages [from (*a*) to (*h*)] are $T/8$ apart in time, T being the period of the forcing. Each snapshot shows the profile (solid curve) predicted using the viscid theory (this study), the profile (dashed curve) predicted using the inviscid theory (Helfrich 1995) and the profile (visualized by the black-and-white boundary of the photo) from laboratory experiments (Helfrich 1995).

sensitive to them. Comparison with Helfrich's (1995) results shows that the inclusion of viscous effects improves the comparison between predicted and observed interface positions (figure 3*a–h*). This is particularly true when either the upper or lower layer becomes thinner than approximately 25 % of the total flow depth, which is, of course, when we would expect viscous effects to be more important.

Nevertheless, discrepancies between the frictional predictions and the observed interface profiles remain. Prominent instabilities form on the interface, consistent with predictions of high values of $|\Delta u|$ for a large portion of the tidal cycle (figures 3*c*, *d* and 3*f*, *g*). Long's (1956) criterion is violated towards the right-hand end of the channel during the first half of the tidal cycle, and towards the left-hand end of the channel during the second half of the tidal cycle. Another discrepancy is the apparent re-entry of mixed fluid from the right-hand end of the channel (figure 3*f*, *g*). This end effect is more prominent than otherwise might have been the case, because the laboratory channel is relatively short, $|x| \leqslant 0.5$. Overall, the frictional solution yields smooth profiles that match the observations well.

4.2. *Flow rates*

In the present study we examine the exchange flow rate in each layer averaged over a forcing cycle. We evaluate the exchange flow at the narrowest section of the channel, using

$$\overline{q}_j = \frac{1}{T}\int_t^{t+T} u_j y_j \, \mathrm{d}t, \quad at\ x = 0. \tag{4.1}$$

For periodic forcing, $\overline{q}_2 = -\overline{q}_1$. To facilitate comparison we use

$$q_e = \frac{\overline{q}_1}{q_{inv}}, \tag{4.2}$$

where $q_{inv} = 0.25$ is the steady inviscid exchange flow rate (Armi 1986). To reveal the dependency of q_e on α, β and γ, we solve (2.6) and (2.7), evaluate q_e and present the results as a series of plots, where one parameter is held constant and the other two are varied. This will enable comparison with the results of Armi (1986), Armi & Farmer (1986), Helfrich (1995) and Zaremba *et al.* (2003).

4.2.1. *Effects of varying β and γ while α is held constant*

The highest predicted exchange flows are for inviscid flow ($\alpha = 0$) subject to barotropic forcing with a period that is very long compared to the travel time through the channel ($\gamma \to \infty$). This case was studied by Armi & Farmer (1986), who found that for $\beta \leqslant \beta_c = 0.544$, the exchange flow rate is not enhanced by the forcing; whereas for $\beta > \beta_c$, the exchange rate increases linearly with increasing β.

In the presence of low friction ($\alpha \leqslant 0.1$) the effect of varying β remains qualitatively the same as in the inviscid case (figure 4*a*), the main difference being that q_e is reduced slightly. For $\beta \to 0$, the solution approaches the steady prediction of Zaremba *et al.* (2003). For $0 < \beta \leqslant \beta_c$, q_e remains essentially unaltered by variations in β and γ. For $\beta > \beta_c$, q_e increases with both increasing β and γ in qualitatively the same manner as predicted by Helfrich (1995).

As friction is increased the exchange rate decreases, and there is an increasing variation in q_e with β and γ for $\beta \leqslant \beta_c$ (figure 4*b*–*d*). An interesting feature of flows with strong friction is that when the forcing period is relatively short the exchange rate can be less than that in the unforced case, i.e. $q_e < q_{Z03}$ where q_{Z03} is the exchange rate predicted by Zaremba *et al.* (2003). This phenomenon, which we will call 'tidal inhibition', is not evident in the inviscid model of Helfrich (1995). It occurs when the combination of relatively high-frequency tidal forcing and friction reduces the exchange rate more than friction acting alone. The variation of upper layer thickness, velocity and flow rate for a tidally inhibited flow is presented in figure 5. The phase lag between the fluctuations in velocity and layer thickness is greater in tidally inhibited

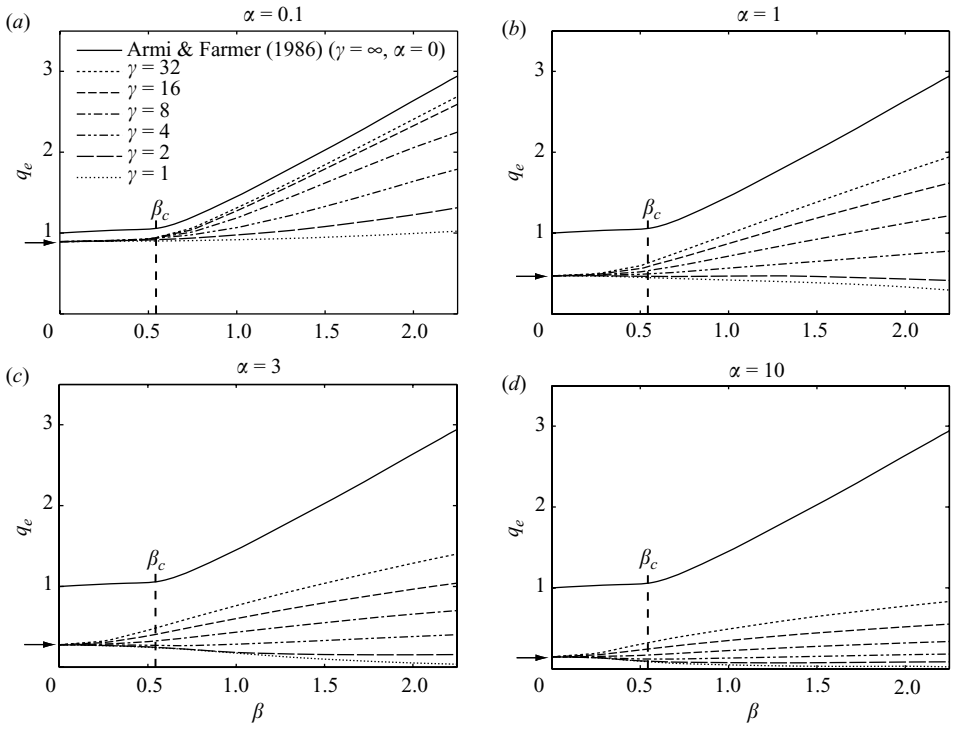

FIGURE 4. Curves of average exchange rate, q_e [see (4.2)], as a function of forcing amplitude β for a range of values of forcing period γ. (*a*) $\alpha = 0.1$, low friction; (*b*) $\alpha = 1$, moderate friction; (*c*) $\alpha = 3$, high friction; (*d*) $\alpha = 10$, very high friction. The inviscid quasi-steady prediction ($\alpha = 0$ and $\gamma = \infty$ in Armi & Farmer 1986) is shown for comparison. The arrows indicate the predictions of Zaremba *et al.* (2003).

flows than in tidally enhanced flows, i.e. flows with $q_e > q_{Z03}$. Tidal inhibition is strongest for $\gamma \approx 1$ (see figure 6).

4.2.2. *Effects of varying α and γ while β is held constant*

The above results show the consistency between the predictions of Armi & Farmer (1986), Helfrich (1995), Zaremba *et al.* (2003) and those of the present study. To further confirm this consistency we set $\beta = 1$ and allow γ to vary while setting $\alpha = 0.1$, 1 and 10 (figure 6). All else being equal, the exchange rate drops as friction is increased. For all values of α the predictions for $\gamma = 0$ match those of Zaremba *et al.* (2003). For $\alpha = 0.1$ the variation of q_e with γ is qualitatively the same as Helfrich (1995), the quantitative difference being a reduction of q_e by approximately 10 %. For $\alpha = 1$ and 10 tidal inhibition is observed for small values of γ.

4.2.3. *Effects of varying α and β while γ is held constant*

Another useful way to visualize the factors influencing the exchange rate is to plot contours of q_e on the α–β plane for specific values of γ. Examples with $\gamma = 2, 4, 8$ and 16 are shown in figure 7(*a–d*). The α–β plane can be separated into two regions, a friction-dominated region where $q_e < 1$, and a forcing-dominated region where $q_e > 1$. The flow is dominated by forcing at high β and low α, as we would expect. Also the region of the α–β plane dominated by forcing increases. The friction-dominated region can be further divided into tidally enhanced ($q_e > q_{Z03}$), and tidally inhibited

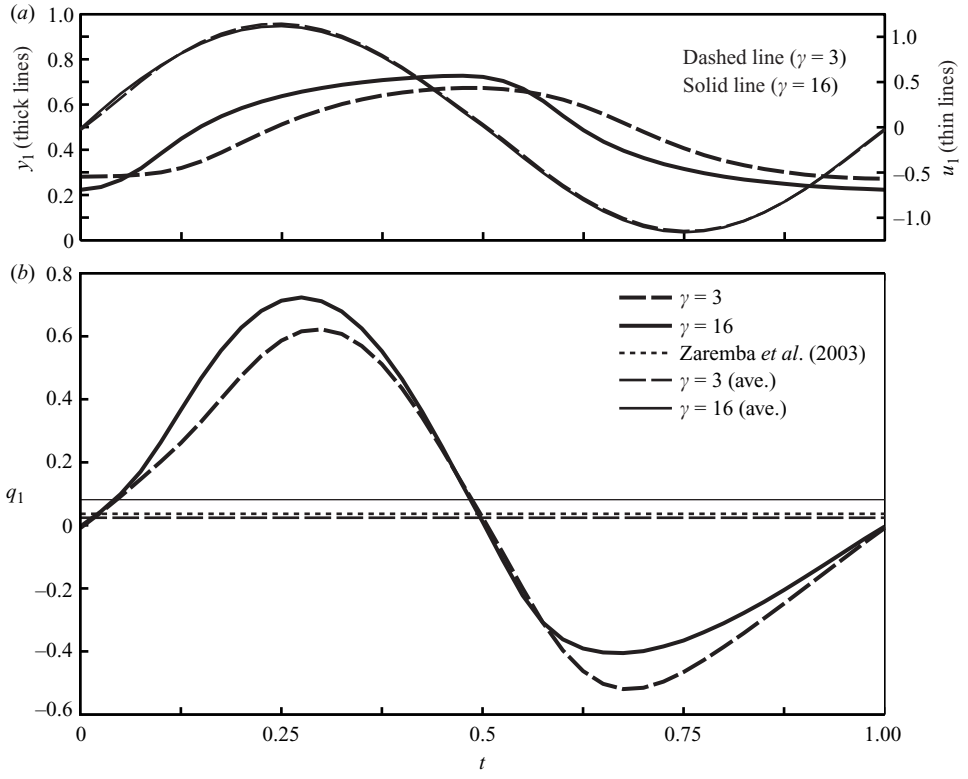

FIGURE 5. (*a*) Time series of upper-layer thickness (y_1) and velocity (u_1). (*b*) Time series of volumetric transport (q_1). The predictions are made at the narrows ($x = 0$), for the combined condition of strong friction ($\alpha = 10$) and moderate barotropic forcing ($\beta = 1$). For $\gamma = 3$, the q_1 average over the forcing period (the thin dashed line in panel *b*) is below the steady, viscous prediction of Zaremba *et al.* (2003) (the dotted line in panel *b*), indicating tidal inhibition. For $\gamma = 16$, the q_1 average over the forcing period (the thin solid line in panel *b*) is above the prediction of Zaremba *et al.* (2003), indicating tidal enhancemeant.

flow ($q_e < q_{Z03}$). Tidally inhibited flow occurs at high α and low γ, and is apparent in figure 7(c, d). The region of tidally inhibited flow disappears at high γ (figure 7a, b), since the phase lag decreases as the tidal period increases.

In summary, we can identify three regimes of exchange flow through a contraction

(1) Forcing-dominated flow ($q_e > 1$)

(2) Tidally enhanced friction-dominated flow ($q_{Z03} < q_e < 1$) and

(3) Tidally inhibited friction-dominated flow ($q_e < q_{Z03}$).

In the following section we will consider whether these flow regimes might be expected in various sea straits.

5. Discussion

Estimates of α, β and γ and several important sea straits are presented in table 1. In compiling table 1 we have used the estimates presented by Helfrich (1995) except for Gibraltar, where we have added a sill, and the Bab el Mandab, where we have used the values suggested by D. A. Smeed (2004; personal communication, 2007). For each strait we have assumed a bottom friction factor $f_b = 0.004$, which corresponds

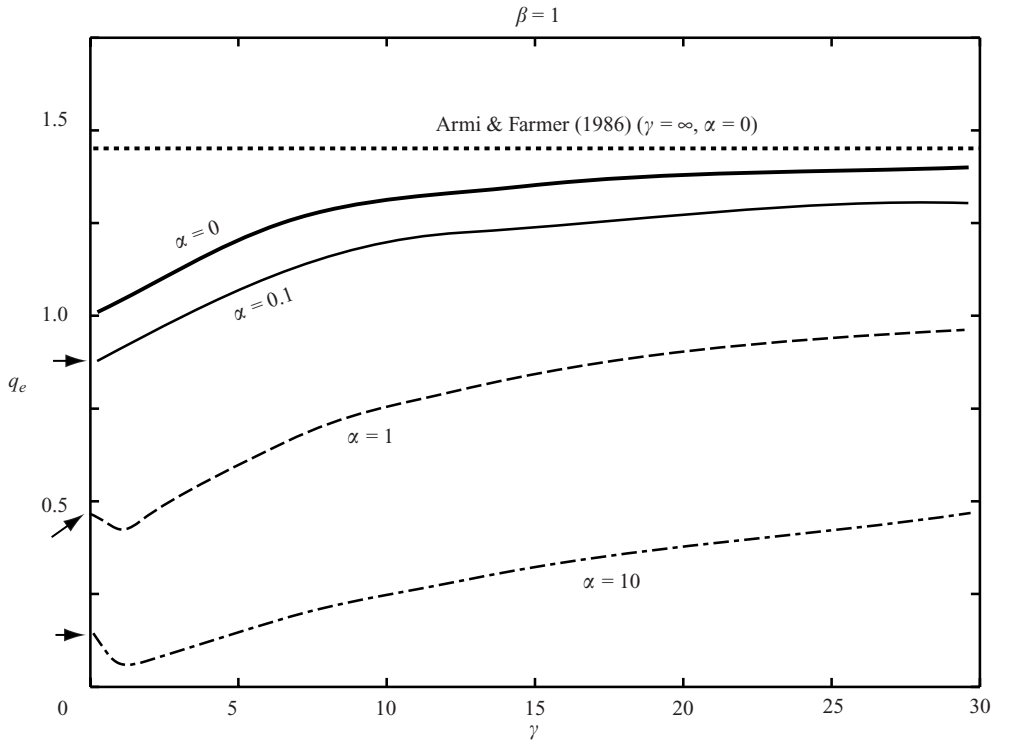

FIGURE 6. Curves of average exchange rate q_e [see (4.2)], as a function of forcing period γ, showing increases in q_e with larger γ under all friction conditions (except the case of short forcing period and strong friction, as illustrated in figure 5). The arrows indicate the predictions of Zaremba *et al.* (2003). The curves approach the inviscid, unsteady solution (Helfrich 1995), as friction diminishes.

to the value determined from field data obtained in the Burlington Ship Canal by Lawrence *et al.* (2004), and is representative of previously published estimates.

While the model presented above accounts for the effects of friction and periodic forcing, there are a number of potentially important factors that it does not consider. The model assumes that the geometry of the strait conforms to our very simple model, that the tidal forcing is of constant amplitude and period, and that the reservoirs on either side of the strait are of infinite extent and uniform density. The model also neglects mixing between the layers, and Coriolis and non-hydrostatic effects.

Three non-dimensional exchange rates are listed in table 1. Under q_{FA86} we list the inviscid steady exchange rates given in Farmer & Armi (1986). We then list q_{Z03}, corresponding to frictional steady flow. Finally we list our predictions for q_e, the exchange rate when both friction and periodic forcing are included. These predictions are subject to all of assumptions listed above. Our goal is not to provide accurate estimates of the exchange rate through any of the straits, but rather to provide a sense of the importance of friction and tidal forcing through comparisons of q_{FA86}, q_{Z03} and q_e.

In Tiran Strait a lower layer of dense Gulf of Aqaba water flows southwards into the Red Sea, and an upper layer of less density Red Sea water flows northwards into the gulf (figure 8*a*). The strait is dynamically short so that frictional effects on the exchange are weak; similarly the tidal forcing is weak, so that the predicted exchange rate is only slightly less than steady inviscid result (table 1).

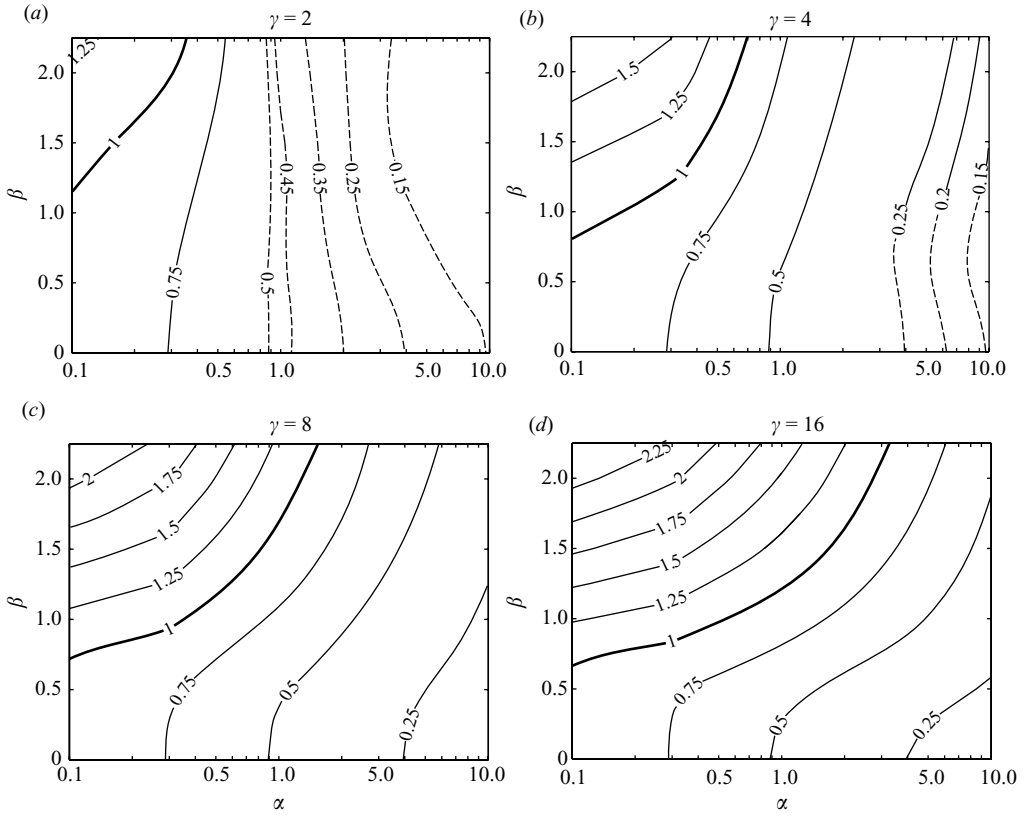

FIGURE 7. Contours of average exchange rate q_e on the α–β plane. (*a*) $\gamma = 2$, (*b*) $\gamma = 4$, (*c*) $\gamma = 8$, (*d*) $\gamma = 16$. In (*a*) and (*b*) the regions with dashed contours indicate tidal inhibition.

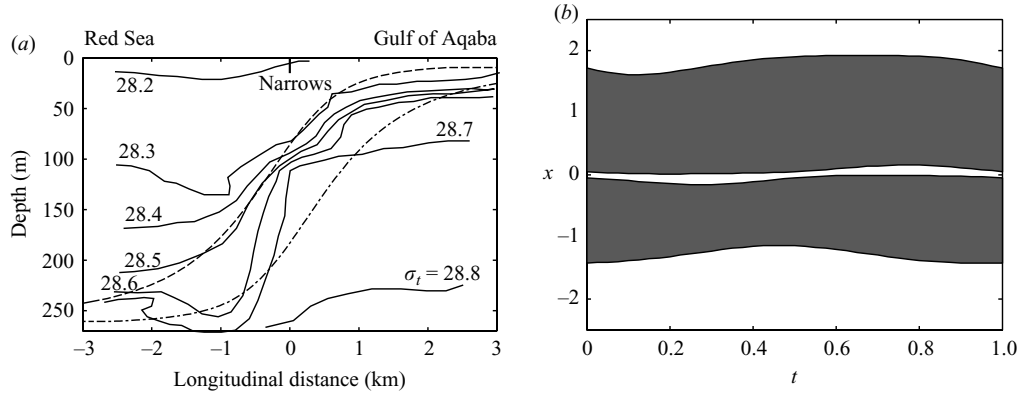

FIGURE 8. (*a*) A vertical section of the Tiran Strait, showing the tidally averaged position of the fluid density structure based on field measurements (solid curves, from Murray *et al.* 1984), and the tidally induced back and forth excursion (the dashed curve and the dashed-dotted curve) of the density interface based on our prediction. (*b*) Conditions under which supercritical (shaded) and subcritical (unshaded) flows are predicted in Tiran Strait as a function of position along the contraction and time (normalized by the tidal period).

Field measurements (Murray, Hecht & Babcock 1984) provide the mean position of density contours (solid curves, figure 8*a*), after removing the tidally induced back and forth excursion of the density structure. Interface positions predicted using the parameter values for the Tiran Strait are in good agreement with the interface measurements. Flooding tides accelerate the upper layer and depress the density interface, whereas ebbing tides accelerate the lower layer and raise the interface. The observed density structure appears to be bounded by the predicted peak flood and ebb interface limits.

Tiran Strait provides a good example of a maximal exchange flow with a region of subcritical flow bounded on both sides by supercritical flow (figure 8*b*). The supercritical regions are not of the same extent, because friction is applied to the bottom, but not at the free surface. While conditions remain similar throughout the tidal cycle there are variations in the extent of the subcritical and supercritical regions. The region of subcritical flow is narrow because of the low value of the friction parameter ($\alpha = 0.04$). As α vanishes, so does the subcritical region, until the inviscid result of critical flow at the narrows ($x = 0$) surrounded by supercritical flow is retrieved.

Maximal exchange flow, as observed in Tiran Strait may be the exception rather than the rule. As α is increased the subcritical region expands, the supercritical regions get smaller, and the tidal variations larger. Eventually, one of the supercritical regions is lost and the flow becomes submaximal for part of the tidal cycle. The period of submaximal flow then increases until maximal flow is lost throughout the entire tidal cycle. As α is increased further, periods of uncontrolled flow appear, and eventually the flow is subcritical throughout the tidal period. The transition from maximal exchange to subcritical flow has been analysed for steady frictional flow in Zaremba *et al.* (2003).

The Strait of Gibraltar exhibits hydraulic control in the vicinity of the Camarinal Sill, but presence of hydraulic control in the Tarifa Narrows is a matter of debate (Armi & Farmer 1988; Garrett, Bormans & Thompson 1990; Sannino, Bargagli & Artale 2004). Thus, depending on conditions in Tarifa Narrows the exchange is either maximal or submaximal. Either way, any model of the Strait of Gibraltar should include the Camarinal Sill. We have added a sill to our geometry using the approximation of Helfrich (1995) that the total depth (560 m) is double the depth of the sill (280 m); however to better reflect the actual width variation (see Sannino *et al.* 2004), we have set the ratio of the width of the channel at the Narrows to the width at the sill to 0.8, rather than 0.5. With this idealization, the flow at Tarifa Narrows is predicted to vary between subcritical and critical during the tidal cycle (figure 9*b*), indicating that the flow alternates between submaximal and maximal exchange.

Predictions of interface level variation at Tarifa Narrows are compared with the observations of Armi & Farmer (1988) in figure 9(*a*). The model provides a reasonable estimate of the asymmetry of the tidal variation in interface level, and of the magnitude of this variation [$O(100\,\mathrm{m})$]. The predicted steepening of the interface between 4:00 and 5:00 and between 16:00 and 17:00 (see figure 9) coincides with the arrival of packets of large amplitude internal waves at Tarifa Narrows. These disturbances are generated at the Camarinal Sill and propagate through the strait (Armi & Farmer 1988).

In general, the predicted interface level falls below the observed level. This is not surprising when we consider that the strait does not have a rectangular cross-section, and that the lower narrower layer is active at the Camarinal Sill; whereas, the upper wider layer is active at Tarifa Narrows. Therefore, the rectangular cross-section

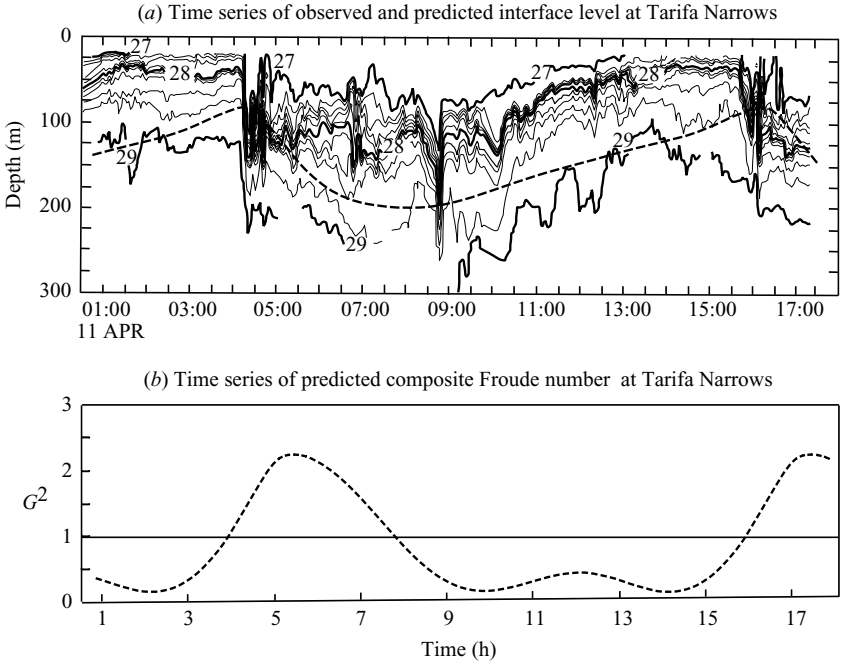

FIGURE 9. (*a*) Time series of the observed and predicted density interface position at Tarifa Narrows together with the $\sigma_t = 27$, 28 and 29 isopycnals, from Armi & Farmer (1988). (*b*) Variation of the composite Froude number with tidal phase.

assumed in the model is under representing the relative channel width at Tarifa Narrows, and the upper layer thickness is overpredicted. Other effects may also be present, for instance our estimates of the friction factors may be too high resulting in a thicker upper layer at Tarifa narrows also.

For the case of an offset sill and contraction Farmer & Armi (1986) calculate the inviscid unforced flow to have an exchange rate $q_{FA86} = 0.73$. Thus, from table 1 the flow is frictionally dominated with tidal enhancement. The inclusion of friction reduces the predicted flow by 33 % to $q_{Z03} = 0.49$, and the inclusion of periodic forcing increases the predicted flow by 27 % to $q_e = 0.62$. The latter prediction is consistent with the predicted tidal enhancement of about 30 % obtained by Sannino *et al.* (2004) in their study of tidal exchange through the strait using a three-dimensional ocean model.

Both Lombok Strait and the Bab el Mandab are subject to moderate friction and weak forcing ($\beta < \beta_c$). In each case the predicted reduction in flow rate due to friction is approximately 40 %, and the increase in flow rate due to tidal enhancement less than 5 %. For the parameter values corresponding to these straits we predict that the flow is submaximal throughout the tidal cycle. The field measurements of Pratt *et al.* (2000) confirm this result for the Bab el Mandab.

The only tidally dominated strait listed in table 1 is Messina. If friction ($\alpha = 0.5$) is considered alone, the flow is reduced to $q_{Z03} = 0.63$; however, when tidal forcing ($\beta = 2$, $\gamma = 4$) is added the flow rate is almost doubled to $q_e = 1.12$, by far the highest of all the straits considered.

Two straits, Oslofjord and the Bosphorus are dynamically long. The flow rates are reduced by approximately 70 % due to friction alone, and are further reduced by

tidal inhibition, although in the case of the Bosphorus tidal inhibition is weak. The exchange flow rate is likely even further reduced in these long straits as they are subject to substantial mixing from various sources as the flow passes through the strait. Field measurements in the Bosphorus show that the density of the fluid in each of the layers changes significantly along the strait (Ozsoy *et al.* 2001).

In summary, our model predicts that, for the idealized geometry that we have assumed, and the parameter sets of the seven straits listed in table 1: one, Tiran, is essentially unaffected by friction and barotropic forcing; three, Lombok, Bab el Mandab and Bosphorus, are substantially influenced by friction, but not barotropic forcing; two, Gibraltar and Messina are substantially influenced by friction and tidal enhancement; and one, the Oslofjord, is substantially influenced by friction and tidal inhibition. Thus, even given the limitations of the hydraulic approach adopted in this paper, it appears that in addition to friction, both tidal enhancement and tidal inhibition can be important in natural straits.

6. Conclusions

A model of frictional periodically forced exchange through a simple contraction was developed based on the equations of internal hydraulics. We explored the effects of variations in friction α and the strength β and period γ of barotropic forcing, on interface elevation, layer velocities and volumetric transport. In the appropriate limits, the results for steady inviscid flow (Armi 1986), quasi-steady inviscid flow (Armi & Farmer 1986), periodically forced inviscid flow (Helfrich, 1995) and steady flow with friction (Zaremba *et al.* 2003) were all recovered. The predicted time-dependent interface position compared well with laboratory experiments of Helfrich (1995).

Increasing friction always reduces the layer velocities and the time-averaged exchange rate. Barotropic forcing usually enhances the exchange rate, and is more effective when its period is longer. However, a weak barotropic forcing with a relatively high frequency can inhibit the exchange rate if the phase lag between the interface position and the layer velocities is sufficiently large.

We did not attempt to model the effects of complicated geometry and forcing, nor did we attempt to model mixing between the layers, and so could not expect to model all the details of flow in sea straits. Nevertheless, we were able to examine whether or not friction and tidal forcing are likely to be important in a series of seven prominent sea straits: Tiran, Gibraltar, Lombok, Messina, Bab-el-Mandeb, Oslofjord and Bosphorous. Together these straits cover a parameter space that includes flows that are unaffected by friction and tidal forcing and flows that are strongly affected by friction and either tidal enhancement or tidal inhibition. The degree of hydraulic control (maximal, submaximal or uncontrolled) varies from strait to strait, and can vary within a given strait during the tidal cycle.

Financial assistance from the Natural Sciences and Engineering Research Council of Canada and the Canada Research Chair program are gratefully acknowledged. We are indebted to three anonymous reviewers for their helpful comments.

REFERENCES

Armi, L. 1986 The hydraulics of two flowing layers with different densities. *J. Fluid Mech.* **163**, 27–58.

Armi, L. & Farmer, D. 1986 Maximal two-layer exchange flow through a contraction with barotropic net flow. *J. Fluid Mech.* **164**, 27–51.

Armi, L. & Farmer, D. M. 1988 The flow of Mediterranean Water through the Strait of Gibraltar. *Progr. Oceanogr.* **21**, 1–105. doi:10.1016/0079-6611(88)90055-9.

Chung, T. J. 2002 *Computational Fluid Dynamics*. Cambridge University Press.

Drazin, P. G. & Reid, W. H. 1981 *Hydrodynamic Stability*. Cambridge University Press.

Farmer, D. & Armi, L. 1986 Maximal two-layer exchange over a sill and through the combination of a sill and contraction with barotropic flow. *J. Fluid Mech.* **1**64, 53–76.

Farmer, D. M. & Armi, L. 1988 The flow of Atlantic Water through the Strait of Gibraltar. *Progr. Oceanogr.* **21**, 1–105. doi:10.1016/0079-6611(88)90055-9.

Frankcombe, L. M. & Hogg, A. M. 2007 Tidal modulation of two-layer hydraulic exchange flows. *Ocean Sci.* **3**, 179–188.

Garrett, C., Bormans, M. & Thompson, K. 1990. Is the exchange through the Strait of Gibraltar maximal or sub-maximal? In *The Physical Oceanography of Sea Straits* (ed. J. Pratt), pp. 271–294. Kluwer.

Gregg, M. & Ozsoy, E. 2002 Flow, water mass changes, and hydraulics in the Bosphorus. *J. Geophys. Res.* **107**, 1–2. 10.1029/2000JC000485.

Helfrich, K. R. 1995 Time-dependent two-layer hydraulic exchange flows. *J. Phys. Oceanogr.* **25**, 359–373.

Hogg, A. M., Ivey, G. N. & Winters, K. B. 2001 Hydraulics and mixing in controlled exchange flows. *J. Geophys. Res.* **106**, 959–972.

Jarosz, E., Murray, S. P. & Inoue, M. 2005 Observations on the characteristics of tides in the Bab el Mandab Strait. *J. Geophys. Res.* **110**, C03015. doi:10.1029/2004JC002299.

Koop, G. C. & Browand, F. K. 1979 Instability and turbulence in a stratified fluid with shear. *J. Fluid Mech.* **9**3, 135–159.

Lawrence, G. A. 1990 On the hydraulics of Boussinesq and non-Boussinesq two-layer flows. *J. Fluid Mech.* **215**, 457–480.

Lawrence, G., Pieters, R., Zaremba, L., Tedford, T., Gu, L., Greco, S. & Hamblin, P. 2004 Summer exchange between Hamilton Harbour and Lake Ontario. *Deep-Sea Res.* **51**, 475–487.

Long, R. R. 1956 Long waves in a two-fluid system. *J. Meteor.* **13**, 70–74.

Morozov, E. G., Trulsen, K., Velarde, M. G. & Vlasenko, V. I. 2002 Internal tides in the Strait of Gibraltar. *J. Phys. Oceanogr.* **32**, 3193–3206.

Murray, S. P., Hecht, A. & Babcock, A. 1984 On the mean flow in the Tiran Strait in winter. *J. Mar. Res.* **42**, 265–287.

Oguz, T., Ozsoy, E. & Latif, M.A. 1990 modelling of hydraulically controlled exchange flow in the Bosporus Strait. *J. Phys. Oceanogr.* **20**, 945–965.

Orlanski, I. 1976 A simple boundary condition for unbounded hyperbolic flows. *J. Comput. Phys.* **21**, 251–269.

Ottensen-Hansen, N. & Moller, J. 1990 Zero blocking solution for the Great Belt Link. In *The Physical Oceanography of Sea Straits* (ed. L. Pratt), pp. 153–170. Kluwer.

Ozsoy, E., Di Iorio, D., Gregg, M. C. & Backhaus, J. O. 2001 Mixing in the Bosphorus Strait and the Black Sea continental shelf: observations and a model of the dense water outflow. *J. Mar. Syst.* **31**, 99–135.

Pratt, L. J., Deese, H. E., Murray, S. P. & Johns, W. 2000 Continuous dynamical modes in Straits having arbitrary cross-sections, with applications to the Bab el Mandab. *J. Phys. Oceanogr.* **30**, 2515–2534.

Sannino, G., Bargagli, A. & Artale, V. 2004 Numerical modelling of the semidiurnal tidal exchange through the Strait of Gibraltar. *J. Geophy. Res.* **109**, C05011. 1–23. doi:10.1029/2003JC002057.

Smeed, D. A. 2004 Exchange through the Bab el Mandab. *Deep-Sea Res.* II, **51**, 455–474.

Winters, K. B. & Seim, H. E. 2000 The role of dissipation and mixing in exchange flow through a contracting channel. *J. Fluid Mech.* **407**, 265–290.

Zaremba, L. J., Lawrence, G. A. & Pieters, R. 2003 Frictional two-layer exchange flow. *J. Fluid Mech.* **474**, 339–354.

Zhu, D. Z. & Lawrence, G. A. 2000 Hydraulics of exchange flows. *J. Hydr. Engng ASCE* **126**, 921–928.